Check for updates

Received: 3 January 2023 | Revised: 29 June 2023 | Accepted: 26 November 2023

DOI: 10.1002/mp.16887

RESEARCH ARTICLE

MEDICAL PHYSICS

CT number calibration audit in photon radiation therapy

Minoru Nakao[1,2,3,4] | **Shuichi Ozawa**[1,2,3,4] | **Hideharu Miura**[1,2,3] | **Kiyoshi Yamada**[1,3] | **Masahiro Hayata**[1,3] | **Kosuke Hayashi**[1,3] | **Daisuke Kawahara**[2,3,4] | **Takeo Nakashima**[3,4,5] | **Yusuke Ochi**[3,5] | **Takuro Okumura**[3,5] | **Haruhide Kunimoto**[3,6] | **Atsushi Kawakubo**[3,7] | **Hayate Kusaba**[3,7] | **Hiroshige Nozaki**[3,8] | **Kosaku Habara**[3,8] | **Naoki Tohyama**[4,9] | **Teiji Nishio**[4,10] | **Mitsuhiro Nakamura**[4,11,12] | **Toshiyuki Minemura**[4,13] | **Hiroyuki Okamoto**[4,14] | **Masayori Ishikawa**[4,15] | **Masahiko Kurooka**[4,16] | **Hidetoshi Shimizu**[4,17] | **Kenji Hotta**[4,18,19] | **Masahide Saito**[4,20] | **Masahiro Nakano**[4,21] | **Masato Tsuneda**[4,22] | **Yasushi Nagata**[1,2,3]

[1]Hiroshima High-Precision Radiotherapy Cancer Center, Hiroshima, Japan

[2]Department of Radiation Oncology, Graduate School of Biomedical & Health Sciences, Hiroshima University, Hiroshima, Japan

[3]Technical Support Working Group in Hiroshima High-Precision Radiotherapy Cancer Center, Hiroshima, Japan

[4]Medical Physics Working Group in Japan Clinical Oncology Group - Radiation Therapy Study Group, Tokyo, Japan

[5]Radiation Therapy Section, Department of Clinical Support, Hiroshima University Hospital, Hiroshima, Japan

[6]Radiation Therapy Department, Hiroshima Prefectural Hospital, Hiroshima, Japan

[7]Radiation Therapy Department, Hiroshima City Hiroshima Citizens Hospital, Hiroshima, Japan

[8]Division of Radiology, Hiroshima Red Cross Hospital & Atomic-bomb Survivors Hospital, Hiroshima, Japan

[9]Division of Medical Physics, Tokyo Bay Makuhari Clinic for Advanced Imaging, Cancer Screening, and High-Precision Radiotherapy, Chiba, Japan

[10]Medical Physics Laboratory, Division of Health Science, Graduate School of Medicine, Osaka University, Osaka, Japan

[11]Department of Radiation Oncology and Image-Applied Therapy, Kyoto University, Kyoto, Japan

[12]Department of Advanced Medical Physics, Graduate School of Medicine, Kyoto University, Kyoto, Japan

[13]Division of Medical Support and Partnership, Institute for Cancer Control, National Cancer Center, Tokyo, Japan

[14]Radiation Safety and Quality Assurance Division, National Cancer Center Hospital, Tokyo, Japan

[15]Faculty of Health Sciences, Hokkaido University, Hokkaido, Japan

[16]Department of Radiation Therapy, Tokyo Medical University Hospital, Tokyo, Japan

[17]Department of Radiation Oncology, Aichi Cancer Center Hospital, Aichi, Japan

[18]Radiation Safety and Quality Assurance division, National Cancer Center Hospital East, Chiba, Japan

[19]Particle Therapy Division, Exploratory Oncology Research and Clinical Trial Center, National Cancer Center, Chiba, Japan

[20]Department of Radiology, University of Yamanashi, Yamanashi, Japan

[21]Department of Radiation Oncology, Kitasato University School of Medicine, Kanagawa, Japan

[22]Graduate School of Medicine, Chiba University, Chiba, Japan

This is an open access article under the terms of the Creative Commons Attribution License, which permits use, distribution and reproduction in any medium, provided the original work is properly cited.

© 2023 The Authors. *Medical Physics* published by Wiley Periodicals LLC on behalf of American Association of Physicists in Medicine.

Correspondence
Minoru Nakao, Hiroshima High-Precision Radiotherapy Cancer Center, 3-2-2, Futabanosato, Higashi-ku, Hiroshima, Hiroshima Prefecture, 732-0057, Japan.
Email: nakao@hiprac.jp

Funding information
Japan Agency for Medical Research and Development (AMED), Grant/Award Number: 2031526; National Cancer Center Research and Development Fund, Grant/Award Number: 2020-J-3; Japan Society for the Promotion of Science (JSPS), Grant/Award Numbers: 19K12865, 23K14869

Abstract

Background: Inadequate computed tomography (CT) number calibration curves affect dose calculation accuracy. Although CT number calibration curves registered in treatment planning systems (TPSs) should be consistent with human tissues, it is unclear whether adequate CT number calibration is performed because CT number calibration curves have not been assessed for various types of CT number calibration phantoms and TPSs.

Purpose: The purpose of this study was to investigate CT number calibration curves for mass density (ρ) and relative electron density (ρ_e).

Methods: A CT number calibration audit phantom was sent to 24 Japanese photon therapy institutes from the evaluating institute and scanned using their individual clinical CT scan protocols. The CT images of the audit phantom and institute-specific CT number calibration curves were submitted to the evaluating institute for analyzing the calibration curves registered in the TPSs at the participating institutes. The institute-specific CT number calibration curves were created using commercial phantom (Gammex, Gammex Inc., Middleton, WI, USA) or CIRS phantom (Computerized Imaging Reference Systems, Inc., Norfolk, VA, USA)). At the evaluating institute, theoretical CT number calibration curves were created using a stoichiometric CT number calibration method based on the CT image, and the institute-specific CT number calibration curves were compared with the theoretical calibration curve. Differences in ρ and ρ_e over the multiple points on the curve ($\Delta\rho_m$ and $\Delta\rho_{e,m}$, respectively) were calculated for each CT number, categorized for each phantom vendor and TPS, and evaluated for three tissue types: lung, soft tissues, and bones. In particular, the CT-ρ calibration curves for Tomotherapy TPSs (ACCURAY, Sunnyvale, CA, USA) were categorized separately from the Gammex CT-ρ calibration curves because the available tissue-equivalent materials (TEMs) were limited by the manufacturer recommendations. In addition, the differences in ρ and ρ_e for the specific TEMs ($\Delta\rho_{TEM}$ and $\Delta\rho_{e,TEM}$, respectively) were calculated by subtracting the ρ or ρ_e of the TEMs from the theoretical CT-ρ or CT-ρ_e calibration curve.

Results: The mean ± standard deviation (SD) of $\Delta\rho_m$ and $\Delta\rho_{e,m}$ for the Gammex phantom were -1.1 ± 1.2 g/cm^3 and -0.2 ± 1.1, -0.3 ± 0.9 g/cm^3 and 0.8 ± 1.3, and -0.9 ± 1.3 g/cm^3 and 1.0 ± 1.5 for lung, soft tissues, and bones, respectively. The mean ± SD of $\Delta\rho_m$ and $\Delta\rho_{e,m}$ for the CIRS phantom were 0.3 ± 0.8 g/cm^3 and 0.9 ± 0.9, 0.6 ± 0.6 g/cm^3 and 1.4 ± 0.8, and 0.2 ± 0.5 g/cm^3 and 1.6 ± 0.5 for lung, soft tissues, and bones, respectively. The mean ± SD of $\Delta\rho_m$ for Tomotherapy TPSs was 2.1 ± 1.4 g/cm^3 for soft tissues, which is larger than those for other TPSs. The mean ± SD of $\Delta\rho_{e,TEM}$ for the Gammex brain phantom (BRN-SR2) was -1.8 ± 0.4, implying that the tissue equivalency of the BRN-SR2 plug was slightly inferior to that of other plugs.

Conclusions: Latent deviations between human tissues and TEMs were found by comparing the CT number calibration curves of the various institutes.

KEYWORDS
stoichiometric method, CT calibration, audit, photon radiation therapy, quality assurance

1 | INTRODUCTION

For photon therapy, the computed tomography (CT) number is converted to mass density (ρ) or relative electron density (ρ_e) based on a CT number calibration curve, and the dose distribution in the human body is estimated by calculating the beam delivery in treatment planning systems (TPSs). CT number calibration curves are typically generated using commercial phantoms.[1]

The validity of a CT number calibration curve is important for individual patients in treatment planning and consistent dosimetric evaluations in multicentric clinical trials. Dosimetry audits for inhomogeneity have been conducted using end-to-end tests with slab or anthropomorphic phantoms.[2–5] However, one of the factors that is not always investigated during end-to-end tests is the CT number calibration curve registered in the TPS. There are two reasons why the CT number calibration curve is

24734209, 0, Downloaded from https://aapm.onlinelibrary.wiley.com/doi/10.1002/mp.16987 by IRCCS Centro di Riferimento Oncologi (CRO)- Aviano (Pordenone), Wiley Online Library on [18/01/2024]. See the Terms and Conditions (https://onlinelibrary.wiley.com/terms-and-conditions) on Wiley Online Library for rules of use; OA articles are governed by the applicable Creative Commons License

not adequately investigated. First, it is difficult to identify the cause of dose errors in end-to-end tests, even if the dose error is caused by the CT number calibration curve. Second, because the audit phantoms only are made of a limited number of TEMs, it is impossible to fully reproduce human tissues. For example, the soft tissue phantom used in the end-to-end test is a water equivalent phantom with the ρ of 1.0 g/cm^3, but in the human body, adipose with the ρ of 0.95 g/cm^3 and muscle with the ρ of 1.05 g/cm^3 are the dominant tissue types, and there are differences between the audit phantom and human body tissues. The same applies to the lungs and bones. For example, the lungs have different densities in the inspiratory and expiratory phases, and bones have different densities in the spongy and cortical bones. Because the adipose-to-muscle ratio and body size vary for each patient, the dose errors for deep tumors caused by the CT number calibration error also vary for each patient. Since the accuracy of the dose calculation by the participating institutions provides an accurate assessment of the survival curves for a clinical trial,[6] it is reasonable to verify the inhomogeneous corrections in the TPS by comparing the CT number calibration curves with human tissue. A CT number calibration survey was conducted using TEMs within the European Particle Therapy Network,[7] indicating that CT number calibration curve deviations among various institutes led to dose deviations.[8–11] The tolerance levels of CT number, ρ, and ρ_e in photon radiation therapy have been suggested in guidance documentations[12] and a previous study.[13,14]

The symbols ρ, ρ_e, and stopping-power ratio of TEMs must be consistent with those of human tissues[15]; hence, inconsistencies in the TEMs owing to insufficient material investigation can cause undesirable influences on the CT number calibration audit. In particular, the physical properties of TEMs differ depending on the base material of the mixture, radiation type, and energy.[16] Producing multiple TEMs separately for each radiation type and energy requires considerable cost, time, and effort. In contrast, CT number calibration audit using a stoichiometric method[17–20] flexibly responds to variations in radiation type and its energy, as well as to updates on standard tissue data.[21–24] A CT number calibration audit using a stoichiometric method was established for photon therapy, and a pilot study was conducted in five radiotherapy institutes.[25] In this study, the number of participating institutes, CT scanners, scan conditions, and TPSs were increased, and the inter-institute variations in the CT-ρ and CT-ρ_e calibration curves were evaluated for each phantom vendor and TPS.

This is the first reported study to assess CT number calibration curves for ρ and ρ_e in Japanese photon therapy institutes. Furthermore, we evaluated ρ and ρ_e deviations from human tissues using the TEMs registered in the TPS.

2 | MATERIAL AND METHODS

2.1 | Study design

A CT number calibration audit phantom (200 mm × 200 mm × 40 mm) was developed to validate the CT-ρ and CT-ρ_e calibration curves registered in the TPS. The axial phantom size was between those of the human head and body.[26] A tough lung, tough bone (Kyoto Kagaku, Kyoto, Japan), and water plug were inserted into a water-equivalent phantom (tough water) (Kyoto Kagaku, Kyoto, Japan). An overview of the study design is presented in Figure 1. We sent a questionnaire to the participating institutes to investigate the CT scanner and TPS type. After completing the questionnaire, the audit phantom was delivered to the participating institutes. The phantom was scanned using a CT scanner, following the institute-specific clinical CT scan protocol. CT images and CT-ρ or CT-ρ_e calibration curves registered in the TPS were submitted to the evaluating institute. The institute-specific CT number calibration curves were compared with the theoretical CT number calibration curves (Section 2.2) from the CT images of the audit phantom. After the comparison, an analysis report was sent to the participating institutes.

2.2 | Stoichiometric CT number calibration

Theoretical CT-ρ and CT-ρ_e calibration curves were generated using a stoichiometric CT number calibration method with three free parameters.[25] The stoichiometric CT number calibration method comprised three steps.

1. A set of materials with known ρ and elemental weights was scanned with CT.
2. A multiparameter fit was performed among the ρ, elemental weights, and measured CT numbers.
3. The theoretical CT numbers were calculated using the resulting parameters, known ρ, and elemental weights.

The theoretical CT number was defined for the stoichiometric CT number calibration using a three-parameter fit model, as:

$$H_x = 1000\alpha\left(\frac{\bar{\mu}_x}{\bar{\mu}_{H_2O}} - 1\right), \quad (1)$$

where H_x denotes the CT number of the material, α denotes a free parameter as a scaling correction, $\bar{\mu}_x$ and $\bar{\mu}_{H_2O}$ denote the photon linear attenuation coefficients of the material and water, respectively, averaged over the x-ray spectrum.

The ratio of the photon linear attenuation coefficient relative to water was defined using two free parameters,

24734209, 0, Downloaded from https://aapm.onlinelibrary.wiley.com/doi/10.1002/mp.16987 by IRCCS Centro di Riferimento Oncologi (CRO)- Aviano (Pordenone), Wiley Online Library on [18/01/2024]. See the Terms and Conditions (https://onlinelibrary.wiley.com/terms-and-conditions) on Wiley Online Library for rules of use; OA articles are governed by the applicable Creative Commons License

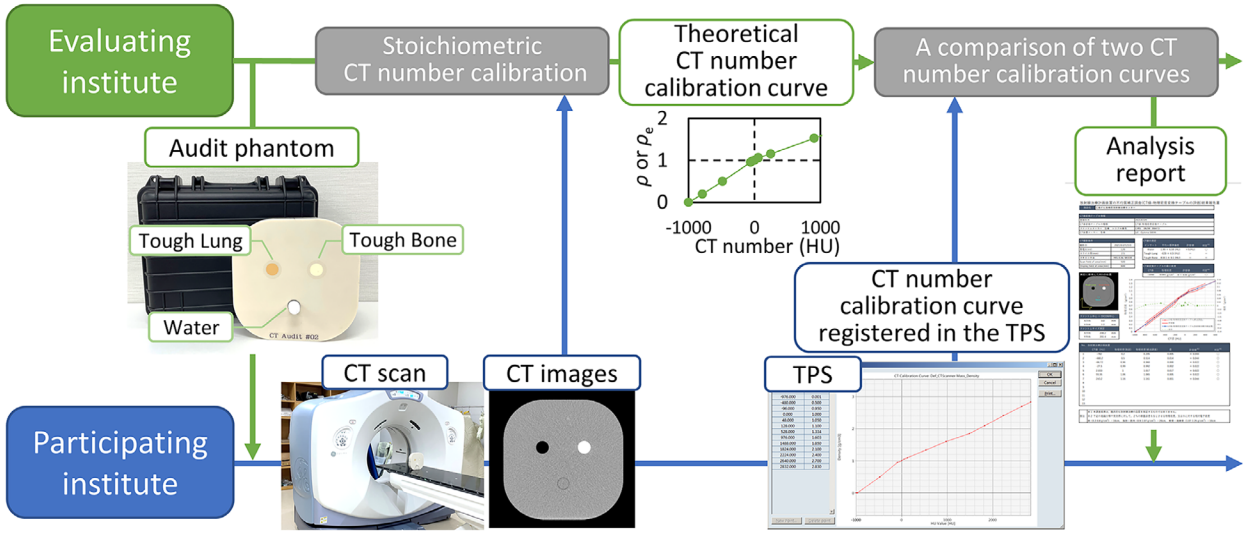

FIGURE 1 Overview of study design.

ρ and elemental weights, as:

$$\frac{\bar{\mu}_x}{\bar{\mu}_{H_2O}}(k_1,k_2)=\frac{\rho_x}{\rho_{H_2O}}\frac{\sum_i (w_i/A_i)\left(Z_i+Z_i^{2.86}k_1+Z_i^{4.62}k_2\right)}{(w_H/A_H)(1+k_1+k_2)+(w_O/A_O)\left(8+8^{2.86}k_1+8^{4.62}k_2\right)}, \tag{2}$$

where ρ_x/ρ_{H_2O} denotes the ratio of the ρ relative to water; i denotes the element index; w_i, A_i, and Z_i denote the elemental weight, atomic mass, and atomic number of index i, respectively; k_1 and k_2 denote the two free parameters; w_H and w_O denote the elemental weights of hydrogen and oxygen, respectively; and A_H and A_O are the atomic masses of hydrogen and oxygen, respectively. Equation (3) shows the least-squares fit to Equations (1) and (2):

$$\sum_n \left[\frac{\bar{\mu}_x}{\bar{\mu}_{H_2O}}(k_1,k_2)_n-\left(\frac{H_x}{1000\alpha}+1\right)_n\right]^2, \tag{3}$$

where n denotes the material index, and a set of tough lung and tough bone with known ρ and elemental weights were used for the least-squares fit. The initial parameters k_1, k_2, and α were 1.24×10^{-3}, 3.06×10^{-5}, and 1.0, respectively. Parameter fit was automatically performed using the general programming language Python, and the open-source SciPy Python package (http://www.scipy.org) was used to minimize Equation (3). The theoretical CT numbers were calculated by substituting the resultant values of k_1, k_2, and α into Equation (4):

$$H_t=1000\alpha\left(\frac{\rho_x}{\rho_{H_2O}}\frac{\sum_i (w_i/A_i)\left(Z_i+Z_i^{2.86}k_1+Z_i^{4.62}k_2\right)}{(w_H/A_H)(1+k_1+k_2)+(w_O/A_O)\left(8+8^{2.86}k_1+8^{4.62}k_2\right)}-1\right), \tag{4}$$

TABLE 1 The symbol ρ and elemental weights for tough lung and tough bone.[28]

	Tough lung	Tough bone	Method
ρ (g / cm^3)	0.374	1.510	(a)
w_H (%)	5.74	5.05	(b)
w_C (%)	62.87	42.14	(b)
w_N (%)	Not detected	0.64	(b)
w_O (%)	29.58	31.40	(f)
w_{Mg} (%)	Not detected	0.06	(e)
w_{Al} (%)	0.29	0.02	(c)
w_{Si} (%)	1.39	0.03	(c)
w_P (%)	0.01	6.54	(c)
w_S (%)	0.01	0.01	(e)
w_{Cl} (%)	0.03	0.05	(d)
w_K (%)	0.05	Not detected	(e)
w_{Ca} (%)	0.02	14.05	(c)
w_{Fe} (%)	0.01	Not detected	(e)
w_{Sr} [%]	Not detected	0.01	(e)

Note: ρ, mass density; w_H, w_C, w_N, w_O, w_{Mg}, w_{Al}, w_{Si}, w_P, w_S, w_{Cl}, w_K, w_{Ca}, w_{Fe}, and w_{Sr} are element weights of hydrogen, carbon, nitrogen, oxygen, magnesium, aluminum, silicon, phosphorus, sulfur, chlorine, potassium, calcium, iron, and strontium, respectively.

The values are determined by (a) ISO 845–2006[27]; (b) Carbon, hydrogen, and nitrogen (CHN) element analysis. (c) Inductively coupled plasma atomic emission spectroscopy (ICP-AES). (d) Ion chromatography. (e) X-ray fluorescence spectrometry. (f) We calculated the elemental weight as the residual weight.

where H_t denotes the theoretical CT number.

The symbol ρ of the tough lung and tough bone were obtained by dividing the weight by the volume according to ISO-845.[27] The symbol ρ and elemental weights were examined using four analyzers[28] (Table 1). Theoretical CT-ρ and CT-ρ_e calibration curves were created using the standard tissue model defined by Kanematsu et al.[29] (Table 2)

24734209, 0, Downloaded from https://aapm.onlinelibrary.wiley.com/doi/10.1002/mp.16987 by IRCCS Centro di Riferimento Oncologi (CRO) Aviano (Pordenone), Wiley Online Library on [18/01/2024]. See the Terms and Conditions (https://onlinelibrary.wiley.com/terms-and-conditions) on Wiley Online Library for rules of use; OA articles are governed by the applicable Creative Commons License

TABLE 2 Summary of ρ, ρ_e, element weights, and mean residual atomic numbers for 11 representative standard tissues.[29]

Name	ρ (g / cm^3)	ρ_e	w_H (%)	w_C (%)	w_N (%)	w_O (%)	w_P (%)	w_{Ca} (%)	w_{res} (%)	$\bar{Z}_{res}$
Air	0.001	0.001	0.00	0.01	75.52	23.17	0.00	0.00	1.30	18.0
Lung	0.384	0.381	10.3	10.7	3.2	74.6	0.2	0.0	1.0	15.9
Extra Lung	0.80	0.79	10.3	10.7	3.2	74.6	0.2	0.0	1.0	15.9
Fat	0.90	0.91	11.96	76.87	0.00	11.17	0.00	0.00	0.00	–
Adipose/marrow	0.950	0.951	11.40	58.92	0.74	28.64	0.00	0.00	0.30	14.7
Muscle/general	1.049	1.040	10.25	14.58	3.20	70.87	0.21	0.02	0.87	16.8
Miscellaneous	1.090	1.077	9.94	20.90	3.84	63.73	0.45	0.27	0.87	15.5
Heavy spongiosa	1.136	1.115	9.30	39.15	2.22	41.71	2.36	4.60	0.66	14.9
Mineral Bone	1.92	1.784	3.6	15.9	4.2	44.8	9.4	21.3	0.8	13.1
Tooth	2.75	2.518	2.2	9.5	2.9	42.1	13.7	28.9	0.7	12.0
Hydroxyapatite	3.156	2.830	0.20	0.00	0.00	41.14	18.50	39.89	0.00	–

Note: ρ, mass density (MD); ρ_e, relative electron density; w_H, w_C, w_N, w_O, w_P, and w_{Ca} are element weights of hydrogen, carbon, nitrogen, oxygen, phosphorus, and calcium, respectively; w_{res}, residual element weight; $\bar{Z}_{res}$, mean residual atomic number.

TABLE 3 Summary of CT number calibration phantoms, TPSs, CT-ρ or CT-ρ_e conversion, and scan conditions for 24 participating institutes.

Manufacturer	TPS	ρ or ρ_e	Number of CT number calibration curve	Number of scan conditions in clinical use
CIRS	Eclipse, Pinnacle^3, or Raystation	ρ	5	6
	Eclipse or Xio	ρ_e	5	6
Gammex	Eclipse, Pinnacle^3, or Raystation	ρ	17	33
	Eclipse, Monaco, or ViewRay TPS	ρ_e	10	21
	Tomotherapy TPS (Planning Station or Precision)	ρ	7	7

Note: CT, computed tomography; TPS, treatment planning system; ρ, mass density; ρ_e, relative electron density; Eclipse (Varian Medical Systems, Palo Alto, CA, USA); Pinnacle^3 (Philips Medical Systems, Fitchburg, WI, USA); Raystation (RaySearch, Stockholm, Sweden); Xio and Monaco (Elekta, Stockholm, Sweden); ViewRay TPS (ViewRay, Inc., Cleveland, OH, USA); Tomotherapy TPS (ACCURAY, Sunnyvale, CA, USA).

2.3 | Institute-specific CT-ρ and CT-ρe calibration curves

Institute-specific CT-ρ and CT-ρ_e calibration curves were registered in TPS and created with either commercial phantoms, namely the Gammex phantom (Gammex Inc., Middleton, WI, USA) or the computerized imaging reference system (CIRS) phantom (Computerized Imaging Reference Systems, Inc., Norfolk, VA, USA). Institute-specific calibration curves of the Gammex phantom were created using phantom-specific ρ and ρ_e values. In contrast, those of the CIRS phantom were created with default ρ and ρ_e values in the catalog.

2.4 | Analysis

The institute-specific CT number calibration curves were compared with the theoretical CT number calibration curves. A total of 24 Japanese photon therapy institutes participated in this study, and the phantom was scanned using 27 CT scanners. A summary of the types of CT scanners used is provided in the Supplementary Material (Table S1). The sizes of the acquisition and reconstruction field of views (FOVs) were determined individually by each institution.

The CT number calibration phantoms, TPSs, CT-ρ or CT-ρ_e conversions, and number of CT number calibration curves and scan conditions are presented in Table 3. All CT number calibration curves and CT images acquired using clinical practice CT scan protocols were obtained from the participating institutions.

To compare the ρ and ρ_e of each TEM with the theoretical CT number calibration curves, the ρ and ρ_e differences for specific TEMs ($\Delta\rho_{TEM}$ and $\Delta\rho_{e,TEM}$, respectively) were calculated by subtracting the ρ or ρ_e of each TEM from the theoretical CT number calibration curve. The term $\Delta\rho_{TEM}$ and $\Delta\rho_{e,TEM}$ were classified into lung (0.2–0.8 g/cm^3), adipose/muscle (0.9–1.07 g/cm^3), and cartilage/spongy-bone (1.07–1.25 g/cm^3) based on the ρ of TEM, and compared with tolerance levels previously determined.[13,14] The reported tolerance levels of ρ_e differences corresponding to a 2% dose difference are ± 0.044, ± 0.022, and ± 0.044 for lung, adipose/muscle, and cartilage/spongy-bone, respectively;

24734209, 0, Downloaded from https://aapm.onlinelibrary.wiley.com/doi/10.1002/mp.16987 by IRCCS Centro di Riferimento Oncologi (CRO) Aviano (Pordenone), Wiley Online Library on [18/01/2024]. See the Terms and Conditions (https://onlinelibrary.wiley.com/terms-and-conditions) on Wiley Online Library for rules of use; OA articles are governed by the applicable Creative Commons License

TABLE 4 Descriptive statistics for the resultant parameters of k_1, k_2, and α.

Free parameter	Mean ± SD (min—max)
k_1	$1.236\times10^{-3} \pm 9.037\times10^{-5}$ ($9.148\times10^{-4} - 1.385\times10^{-3}$)
k_2	$3.646\times10^{-5} \pm 3.189\times10^{-6}$ ($3.037\times10^{-5} - 4.290\times10^{-5}$)
A	0.986 ± 0.023 (0.934 – 1.071)

Abbreviations: max, maximum; min, minimum; SD, standard deviation.

the tolerance levels of ρ differences are comparable to those of ρ_e differences. In addition, to compare the whole CT number calibration curve, the differences in ρ and ρ_e over multiple points on the curve ($\Delta\rho_m$ and $\Delta\rho_{e,m}$, respectively) were calculated by subtracting the institute-specific CT number calibration curve from the theoretical CT number calibration curve for each CT number. Multipoint $\Delta\rho_m$ and $\Delta\rho_{e,m}$ values were calculated for a pair of two calibration curves and classified into lung, adipose/muscle, or cartilage/spongy bone, based on the ρ corresponding to the CT number. To evaluate $\Delta\rho_m$ and $\Delta\rho_{e,m}$ separately for each phantom vendor (Gammex-ρ, Gammex-ρ_e, CIRS-ρ, and CIRS-ρ_e), the $\Delta\rho_m$ and $\Delta\rho_{e,m}$ were aggregated for each phantom vendor over multiple calibration curves submitted from the participating institutes and compared with the tolerance levels for each tissue type. The CT-ρ calibration curves for Tomotherapy TPSs (ACCURAY, Sunnyvale, CA, USA) were created using the Gammex phantom; however, they were categorized separately from the Gammex CT-ρ calibration curves because the available TEMs were limited by the manufacturer's recommendations.

3 | RESULTS

A summary of CT scanner type and institute-specific clinical CT scan protocol is provided in the Supplementary Material (Table S1). Several institutions reported differing sizes between the acquisition and reconstruction FOVs. Differences in FOV sizes arose due to the specifications of the CT scanner. However, three institutions reported using a reconstruction FOV wider than the acquisition FOV, and five institutions used a reconstruction FOV that was narrower than the acquisition FOV.

The stoichiometric CT number calibration method was applied to 43 CT images acquired from 24 Japanese photon therapy institutes. Negative parameters (unphysical values) were not obtained for the resultant free parameters k_1 and k_2 (Table 4). Figure 2 shows the averaged CT-ρ calibration curve created from 43 CT images of the audit phantom. The minimum and maximum values represent the theoretical CT numbers of standard tissues. According to Equation (4), the variation in theoretical CT numbers near water was negligible, while a significant variation was observed in the regions

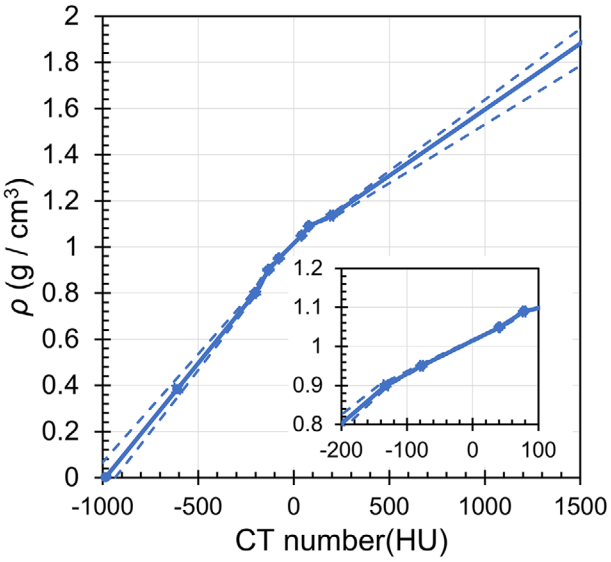

FIGURE 2 Averaged CT-ρ calibration curve created from the CT images of the audit phantom. Dashed lines represent the minimum and maximum values. CT, computed tomography.

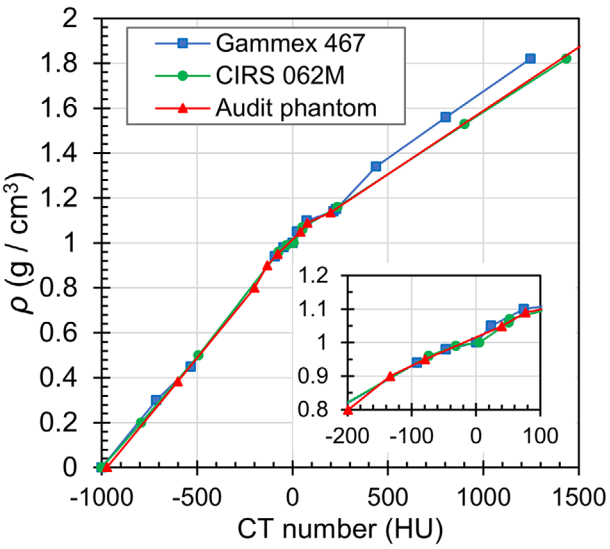

FIGURE 3 Example of CT-ρ calibration curves for Gammex, CIRS, and CT number calibration audit phantom. CT, computed tomography; CIRS, computerized imaging reference systems.

of the lung and bone. The descriptive statistics of CT number and ρ for 11 representative standard tissues[29] are presented in Table 5. The standard deviation (SD), minimum and maximum values of ρ were determined based on Figure 2. Figures 3 and 4 show comparison examples among Gammex, CIRS, and audit phantom for the CT-ρ and CT-ρ_e calibration curves, respectively. Figure 5 presents boxplots of $\Delta\rho_{TEM}$ and $\Delta\rho_{e,TEM}$ for each TEM of the Gammex and CIRS phantoms. The number of CT-ρ calibration curves, CT-ρ_e calibration curves and CT images used to create these boxplots are listed in Table 3. The terms $\Delta\rho_{TEM}$ and $\Delta\rho_{e,TEM}$ in

24734209, 0, Downloaded from https://aapm.onlinelibrary.wiley.com/doi/10.1002/mp.16987 by IRCCS Centro di Riferimento Oncologi (CRO) Aviano (Pordenone), Wiley Online Library on [18/01/2024]. See the Terms and Conditions (https://onlinelibrary.wiley.com/terms-and-conditions) on Wiley Online Library for rules of use; OA articles are governed by the applicable Creative Commons License

TABLE 5 Descriptive statistics (mean ± SD (min – max)) of CT number and ρ, along with the tolerance levels[13,14], for 11 representative standard tissues.[29]

Name	CT number (HU)	ρ (g/cm^3)	Tolerance level (g/cm^3)
Air	−985 ± 23.7 (−1069 – −933)	–	–
Lung	−610 ± 14.6 (−662 – −577)	0.384 ± 0.015 (0.349 – 0.433)	± 0.044
Extra lung	−202 ± 4.8 (−219 – −191)	0.8 ± 0.007 (0.788 – 0.823)	± 0.044
Fat	−133 ± 3.5 (−144 – −129)	0.9 ± 0.003 (0.894 – 0.910)	± 0.022
Adipose/marrow	−78 ± 2.2 (−85 – −75)	0.95 ± 0.002 (0.947 – 0.955)	± 0.022
Muscle/general	41 ± 1.1 (39 – 45)	1.049 ± 0.001 (1.046 – 1.051)	± 0.022
Miscellaneous	78 ± 2.0 (75 – 86)	1.09 ± 0.001 (1.082 – 1.091)	± 0.044
Heavy spongiosa	198 ± 8.3 (186 – 223)	1.136 ± 0.005 (1.128 – 1.144)	± 0.044
Mineral bone	1567 ± 68.5 (1457 – 1762)	1.92 ± 0.038 (1.821 – 1.986)	–
Tooth	3063 ± 134.4 (2846 – 3444)	2.75 ± 0.044 (2.562 – 2.830)	–
Hydroxyapatite	4290 ± 205.2 (3948 – 4845)	3.156 ± 0.068 (2.995 – 3.282)	–

Abbreviations: CT, computed tomography; HU, Hounsfield Unit; max, maximum; min, minimum; SD, standard deviation; ρ, mass density.

% were relative to water (e.g., if ρ_e is 0.3 for lung tissue and $\Delta\rho_{e,TEM}$ is 0.03, $\Delta\rho_{e,TEM}$ in % is 3%). The values of $\Delta\rho_{TEM}$ and $\Delta\rho_{e,TEM}$ varied for the Gammex phantom and were larger than those for the CIRS phantom. The symbols ρ and ρ_e for 30% $CaCO_3$ (CB2), 50% $CaCO_3$ (CB2), and cortical bone (SB3) were systematically larger than those obtained from the theoretical CT number calibration curves of the audit phantom (Figures 3 and 4); thus, the $\Delta\rho_{TEM}$ and $\Delta\rho_{e,TEM}$ were negative values (Figure 5). The descriptive statistics of $\Delta\rho_{TEM}$ and $\Delta\rho_{e,TEM}$ for each TEM are presented in Table 6. The percentages of the TEMs that exceeded the ρ_e tolerance levels were 10.5% (2/19), 66.7% (2/3), and 19% (4/21) in the breast (BR-12), solid water, and brain (BRN-SR2), respectively. In contrast, the percentage of the TEMs that exceeded the ρ tolerance level was 12.1% (4/33) for BRN-SR2. The symbols ρ and ρ_e of the CIRS phantom were single values, while those of the Gammex phantom were presented as ranges (Table 6). For the CIRS phantom, all institutions have registered the same catalog values of the TEMs. Conversely, for the Gammex phantom, most institutions have registered the manufacturer-provided specific ρ and ρ_e values into the TPS. These specific values vary with each serial number.

Figure 6 displays boxplots of $\Delta\rho_m$ and $\Delta\rho_{e,m}$ between the institute-specific CT number calibration curves and

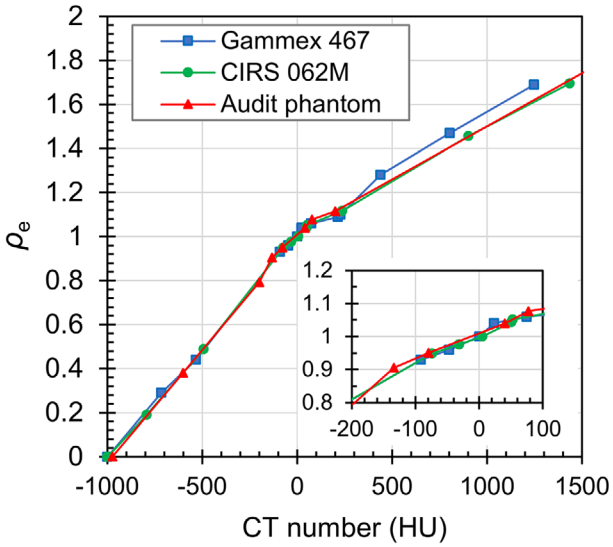

FIGURE 4 Example of CT-ρ_e calibration curves for Gammex, CIRS, and CT number calibration audit phantom. CT, computed tomography; CIRS, computerized imaging reference systems.

the theoretical CT number calibration curves. The number of CT-ρ calibration curves, CT-ρ_e calibration curves and CT images used to create these boxplots are listed in Table 3. The boxplots were constructed by aggregating $\Delta\rho_m$ and $\Delta\rho_{e,m}$ among the participating institutes. The descriptive statistics and tolerance levels for each tissue type are presented in Table 7. Figure 7 depicts a worst-case example of the maximum difference between institute-specific and theoretical CT-ρ calibration curves for Tomotherapy TPS because the $\Delta\rho_m$ of Tomotherapy-TPS-ρ was larger than that of Gammex-ρ for adipose/muscle.

4 | DISCUSSION

The inter-institute variations in the CT-ρ and CT-ρ_e calibration curves of 24 Japanese photon therapy institutes were quantified for the first time. Several institutions reported differing sizes between the acquisition and reconstruction FOVs in the Supplementary Material (Table S1). For radiotherapy planning, it is advantageous to use wide FOV CT images to encompass the patient's entire body. Extended FOV technique is used for planning CT image in three institutions, which allows a wider reconstruction FOV than the acquisition FOV.[30,31] Conversely, in five institutions, the reconstruction FOV is narrower than the acquisition FOV. The variation in CT numbers from the acquisition FOV is larger than that from reconstruction FOV.[32] When the acquisition FOV was adjusted, the collimator of the CT scanner is shifted to minimize unnecessary x-ray exposure. As a result of this shift, the effective energy of the x-rays changes, causing variations in the CT numbers. If only one CT number calibration curve is registered in the TPSs, the

24734209, 0, Downloaded from https://aapm.onlinelibrary.wiley.com/doi/10.1002/mp.16987 by IRCCS Centro di Riferimento Oncolog (CRO)- Aviano (Pordenone), Wiley Online Library on [18/01/2024]. See the Terms and Conditions (https://onlinelibrary.wiley.com/terms-and-conditions) on Wiley Online Library for rules of use; OA articles are governed by the applicable Creative Commons License

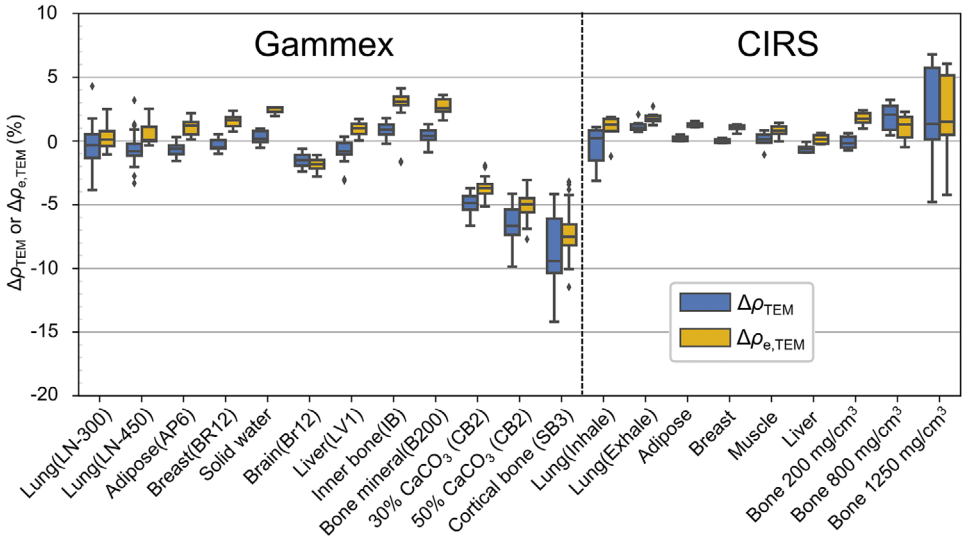

FIGURE 5 Box-and-whisker plot of $\Delta\rho_{TEM}$ and $\Delta\rho_{e,TEM}$ between the audit phantom and each TEM of Gammex and CIRS phantoms. The bottom, middle, and top of the box represent the lower, median, and upper quartiles, respectively. The whiskers extend to the lowest data point, which is within 1.5 times the IQR of the lower quartile, and the highest data point which is within 1.5 times the IQR of the upper quartile. Outliers were defined as those less than 1.5 × IQR of the lower quartile or greater than 1.5 × IQR of the upper quartile. CIRS, Computerized Imaging Reference Systems; IQR, interquartile range.

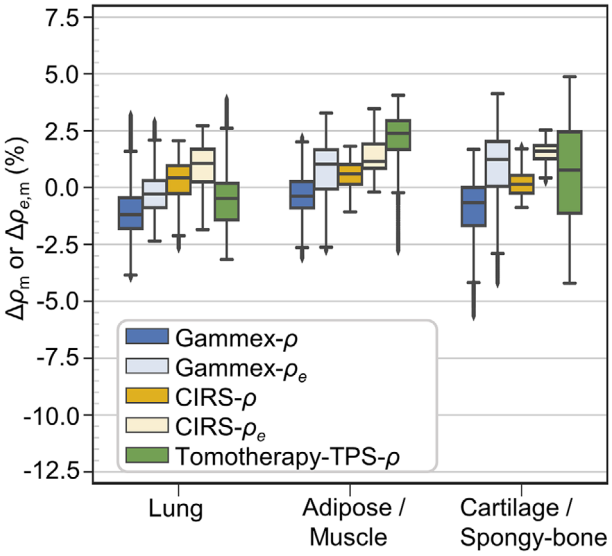

FIGURE 6 Box-and-whisker plot of $\Delta\rho_m$ or $\Delta\rho_{e,m}$ between the CT number calibration curves registered in the TPS and those created using the audit phantoms. The interpretation of the box-and-whisker plots is identical to Figure 5. Gammex-ρ and Gammex-ρ_e represent $\Delta\rho_m$ or $\Delta\rho_{e,m}$ for the Gammex phantom, respectively. CIRS-ρ and CIRS-ρ_e represent $\Delta\rho_m$ or $\Delta\rho_{e,m}$ for the CIRS phantom, respectively. Tomotherapy-TPS-ρ represents $\Delta\rho_m$ for Tomotherapy TPSs. CT, computed tomography; CIRS, Computerized Imaging Reference Systems; TPS, treatment planning systems.

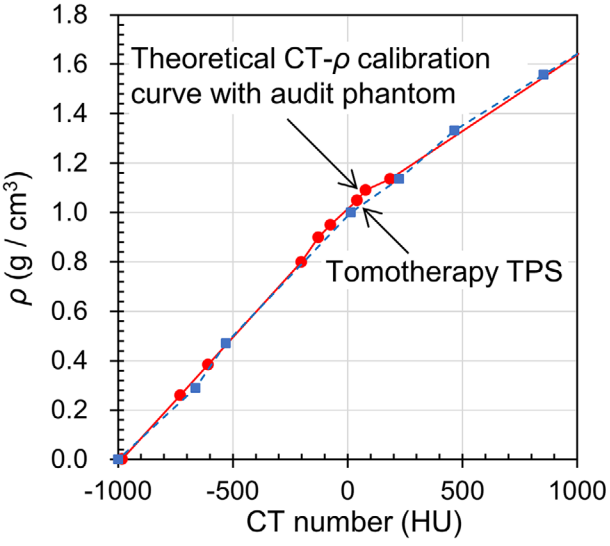

FIGURE 7 Worst-case example of the maximum difference between institute-specific and theoretical CT-ρ calibration curves for Tomotherapy TPS. TPS, treatment planning systems.

variation could potentially cause inaccuracies in the CT number calibration. Therefore, the acquisition FOV is kept constant to minimize the variation of CT numbers, while the reconstruction FOV is varied as required.

CT number calibration curves registered in the TPS were created using either Gammex or CIRS phantoms. The theoretical CT numbers using the stoichiometric CT number calibration method with three free parameters[25,28] were found to be more consistent with the measured CT numbers than conventional methods.[17,18] The standard tissue model[29] presented in Table 2 was established based on International Commission on Radiological Protection Publication 110 (ICRP-110).[24] Therefore, the TEMs of the Gammex and CIRS phantoms were evaluated at a third-party evaluating institute. Figures 3 and 4 show that the CIRS phantom can be considered more equivalent to human tissues than the Gammex phantom in terms of

24734209, 0, Downloaded from https://aapm.onlinelibrary.wiley.com/doi/10.1002/mp.16987 by IRCCS Centro di Riferimento Oncologi (CRO) Aviano (Pordenone), Wiley Online Library on [18/01/2024]. See the Terms and Conditions (https://onlinelibrary.wiley.com/terms-and-conditions) on Wiley Online Library for rules of use; OA articles are governed by the applicable Creative Commons License

TABLE 6 Descriptive statistics (mean ± SD (min – max)) of $\Delta\rho_{TEM}$ and $\Delta\rho_{e,TEM}$ for each TEM of Gammex and CIRS phantoms.

	Mass density			Relative electron density		
	n	ρ (g / cm^3)	$\Delta\rho_{TEM}$ (%)	n	ρ_e	$\Delta\rho_{e,TEM}$ (%)
Gammex						
Lung (LN-300)	40	0.293 ± 0.008 (0.270 – 0.310)	−0.4 ± 1.4 (−3.8 – 4.3)	21	0.286 ± 0.006 (0.281 – 0.300)	0.3 ± 1.0 (−1.0–2.5)
Lung (LN-450)	40	0.468 ± 0.012 (0.440 – 0.490)	−0.6 ± 1.2 (−3.3 – 3.2)	21	0.449 ± 0.011 (0.435 – 0.468)	0.6 ± 0.9 (−0.3 – 2.5)
Adipose (AP6)	34	0.944 ± 0.004 (0.935 – 0.954)	−0.6 ± 0.5 (−1.6 – 0.3)	21	0.927 ± 0.004 (0.924 – 0.937)	1.1 ± 0.7 (0.1 – 2.2)
Breast (BR 12)	33	0.982 ± 0.003 (0.978 – 0.988)	−0.3 ± 0.4 (−1.0 – 0.5)	19	0.961 ± 0.004 (0.956 – 0.965)	1.6 ± 0.5 (0.7 – 2.4)
Solid water	19	1.017 ± 0.002 (1.013 – 1.020)	0.3 ± 0.5 (– 0.5– 1.0)	3	0.990 ± 0.002 (0.988 – 0.991)	2.4 ± 0.3 (2.0 – 2.6)
Brain (SR2)	33	1.051 ± 0.001 (1.049 – 1.053)	−1.5 ± 0.5 (−2.4 – 0.6)	21	1.046 ± 0.003 (1.040 – 1.049)	−1.8 ± 0.4 (−2.8 – −1.1)
Liver (LV1)	33	1.097 ± 0.006 (1.089 – 1.109)	−0.8 ± 0.7 (−3.1 – 0.3)	19	1.068 ± 0.007 (1.059 – 1.081)	0.9 ± 0.5 (0.0 – 1.7)
Inner bone (IB3)	35	1.139 ± 0.006 (1.129 – 1.147)	0.9 ± 0.6 (– 0.2 – 1.8)	19	1.092 ± 0.007 (1.082 – 1.099)	2.8 ± 1.6 (– 1.7– 4.1)
Bone mineral (B200)	34	1.151 ± 0.003 (1.146 – 1.159)	0.4 ± 0.6 (−0.9 – 1.3)	21	1.103 ± 0.003 (1.099–1.110)	2.7 ± 0.6 (1.6 – 3.6)
Bone (CB2-30% $CaCO_3$)	39	1.333 ± 0.002 (1.329 – 1.335)	−4.9 ± 0.7 (−6.6 –3.7)	21	1.276 ± 0.005 (1.265 – 1.279)	−3.7 ± 0.8 (−5.1 – −1.9)
Bone (CB2-50% $CaCO_3$)	40	1.559 ± 0.001 (1.557 – 1.561)	−6.4 ± 1.5 (−9.9 – −4.1)	21	1.468 ± 0.004 (1.460 – 1.471)	−5.1 ± 1.1 (−7.7 – −3.1)
Cortical bone (SB3)	40	1.822 ± 0.001 (1.819 – 1.824)	−8.7 ± 2.8 (−14.2 – −4.2)	21	1.693 ± 0.004 (1.685 – 1.696)	−7.2 ± 2.2 (−11.5 – −3.2)
CIRS						
Lung (inhale)	6	0.2	−0.4 ± 1.6 (– 3.1 – 1.1)	6	0.19	0.4 ± 1.6 (−2.3 – 1.9)
Lung (exhale)	6	0.5	1.2 ± 0.4 (0.7 – 2.1)	6	0.489	1.8 ± 3.5 (1.2 – 2.7)
Adipose	6	0.96	0.2 ± 0.2 (0.0 – 0.5)	6	0.949	1.3 ± 0.2 (1.1 – 1.6)
Breast 50/50	6	0.99	0.0 ± 0.2 (– 0.2 –0.2)	6	0.976	1.0 ± 0.2 (0.6 – 1.3)
Muscle	6	1.06	0.1 ± 0.6 (−1.1 – 0.8)	6	1.043	0.8 ± 0.5 (0.0 – 1.4)
Liver	5	1.07	−0.6 ± 0.3 (−0.9 – −0.1)	5	1.052	0.2 ± 0.4 (−0.2 – 0.6)
Bone 200 mg/cm^3 HA	6	1.16	−0.1 ± 0.5 (−0.7 – 0.6)	6	1.117	1.8 ± 0.5 (1.0 – 2.4)
Bone 800 mg/cm^3 HA	6	1.53	1.9 ± 1.1 (0.5 – 3.2)	6	1.456	1.1 ± 1.0 (−0.5 – 2.3)
Bone 1250 mg/cm^3 HA	5	1.82	1.8 ± 4.2 (−4.8–6.8)	5	1.695	1.8 ± 3.7 (−4.2 – 6.1)

Abbreviations: HA, hydroxyapatite; max, maximum; min, minimum; n, number of CT image sets; SD, standard deviation; TEM, tissue-equivalent material; ρ, mass density; ρ_e, relative electron density.

converting CT numbers into ρ or ρ_e of high-density organs. However, when matching elemental weights between TEMs and human tissues, more careful evaluation is required because the high-density plugs of the CIRS phantom contain barium[20,33] The specific reasons for the discrepancy between the Gammex bone (CB2-30% $CaCO_3$), bone (CB2-50% $CaCO_3$), and cortical bone (SB3) plugs and the theoretical CT-ρ or CT-ρ_e calibration curve of the audit phantom remain unclear. A previous study[34] indicated that the tissue equivalency of these three plugs was superior to that of the bone plugs in the CIRS phantom when using the manufacturer's ρ

24734209, 0, Downloaded from https://aapm.onlinelibrary.wiley.com/doi/10.1002/mp.16987 by IRCCS Centro di Riferimento Oncologi (CRO) Aviano (Pordenone), Wiley Online Library on [18/01/2024]. See the Terms and Conditions (https://onlinelibrary.wiley.com/terms-and-conditions) on Wiley Online Library for rules of use; OA articles are governed by the applicable Creative Commons License

TABLE 7 Descriptive statistics (mean ± SD (min – max)) of $\Delta\rho_m$ and $\Delta\rho_{e,m}$, along with the tolerance levels[13,14], for three tissue types—Namely, lung, adipose/muscle, and cartilage/spongy bone.

Tissue type	ρ (g/cm^3)	Gammex		CIRS		Tomotherapy TPS	Tolerance level
		$\Delta\rho_m$ (%)	$\Delta\rho_{e,m}$ (%)	$\Delta\rho_m$ (%)	$\Delta\rho_{e,m}$ (%)	$\Delta\rho_m$ (%)	
Lung	0.2 – 0.8	−1.1 ± 1.2 (−4.0 – 3.2)	−0.2 ± 1.1 (−2.4 – 2.9)	0.3 ± 0.8 (−2.7 – 2.0)	0.9 ± 0.9 (−1.9 – 2.7)	−0.5 ± 1.3 (−3.2 – 3.9)	± 0.044
Adipose/muscle	0.9 – 1.07	−0.3 ± 0.9 (−3.1 – 2.2)	0.8 ± 1.3 (−2.8 – 3.3)	0.6 ± 0.6 (−1.1 – 1.8)	1.4 ± 0.8 (−0.2 – 3.5)	2.1 ± 1.4 (−2.8 – 4.1)	± 0.022
Cartilage/spongy bone	1.07 – 1.25	−0.9 ± 1.3 (−5.6 – 1.7)	1.0 ± 1.5 (−4.2 – 4.1)	0.2 ± 0.5 (−0.9 – 1.8)	1.6 ± 0.5 (−0.3 – 2.5)	0.7 ± 2.2 (−4.2 – 4.9)	± 0.044

Abbreviations: max, maximum; min, minimum; SD, standard deviation; ρ, mass density; ρ_e, relative electron density; CIRS, Computerized Imaging Reference Systems; TPS, treatment planning systems.

and elemental weights. A compositional analysis of the Gammex phantom could potentially identify the underlying cause. However, unlike tough lung and tough bone, it was not possible to perform a compositional analysis on the Gammex phantoms from the participating institutions in this study.

The tolerance levels,[13,14] corresponding to a 2% dose difference, were previously established considering the worst-case scenario in clinical situations. Because the differences in ρ and ρ_e cause a dose difference as a function of tissue thickness, stricter tolerance levels are set when the effective tissue thickness is larger. Based on the ICRP-110 whole-body voxel phantom,[24] we measured the maximum tissue thicknesses in the axial planes for the lung, adipose/muscle, and cartilage/spongy-bone. We then defined the effective tissue thicknesses as the reasonable target depths at these maximum tissue thicknesses: 10 cm for the lung, 20 cm for adipose/muscle, and 10 cm for cartilage/spongy-bone. The tolerance levels in ρ and ρ_e, considering these effective tissue thicknesses and the tissue maximum ratio of the low effective energy x-ray beam, were defined as ± 0.044 for lung, ± 0.022 for adipose/muscle, and ± 0.044 for cartilage/spongy-bone. The variation CT-ρ calibration curve was compared to the tolerance levels in Table 5. Although there is a large variation in the CT number calibration curves in the region of mineral bone and tooth, the impact on the dose distribution is negligible because the maximum thickness is less than 1 cm in the ICRP-110 phantom. For heavy spongiosa, which has a maximum thickness of 10 cm in the ICRP-110 phantom, the variation range in ρ, defined as the maximum value minus the minimum value, was 0.016 g/cm^3, which is within the tolerance level of ± 0.044 g/cm^3. On the other hand, for lung, the variation range in ρ was 0.084 g/cm^3, which is comparable to the tolerance level of ± 0.044 g/cm^3. This suggests that variations in CT number calibration curves due to the difference in CT scanner type and scan conditions may affect the accuracy of the dose calculation in lungs. In addition, the tolerance level of adipose/muscle is stricter than that of the lung and cartilage/spongy-bone because adipose/muscle is the dominant tissue type in the human body, and the effective tissue thickness is the largest in the pelvic region. Therefore, some TEMs exceeded the tolerance level for adipose and muscle tissues.

Many institutes using the Gammex phantom created a CT-ρ_e calibration curve using the CT number of real water rather than solid water. The average $\Delta\rho_{e,TEM}$ value was 2.4% for solid water (Table 6), which exceeded the tolerance level (± 0.022) for adipose/muscle because the elemental weights of solid water were different from those of a human body tissue.

For some BRN-SR2 plugs, in which both $\Delta\rho_{TEM}$ and $\Delta\rho_{e,TEM}$ exceeded the tolerance level (± 0.022), the average CT number, ρ, and ρ_e values were 18 Hounsfield Unit (HU), 1.052 g/cm^3, and 1.047, respectively. The symbols ρ and ρ_e of the standard human brain are 1.04 g/cm^3 and 1.034, respectively.[23] Furthermore, after the analysis, we sent an additional questionnaire to the radiotherapy institutes that exceeded the tolerance levels, and the measured CT number of the human brain at those institutes was 20–40 HU. The symbols ρ and ρ_e of the BRN-SR2 plug were approximately 1% larger than those of the human brain, whereas the CT number difference was 2–22 HU smaller than that of the human brain. This implies that the tissue equivalency of the BRN-SR2 plug was slightly inferior to that of the other TEMs, as shown in another study comparing theoretical CT numbers with the measured CT numbers of a Gammex phantom.[34]

Although several TEMs of the Gammex phantom exceeded the tolerance levels, the average $\Delta\rho_m$ and $\Delta\rho_{e,m}$ values were lower than the tolerance levels (Table 7). More specifically, the BR-12, solid water, and BRN-SR2 plugs, which exceeded the tolerance level, had a small influence because the CT-ρ and CT-ρ_e calibration curves were created using multiple TEMs for the adipose/muscle (Figures 3 and 4). In contrast, the CT-ρ calibration curve for Tomotherapy was created using a few TEMs and water for the adipose/muscle, and the average $\Delta\rho_m$ value for Tomotherapy-TPS-ρ was larger than those obtained from the other CT number calibration curves. This is because the manufacturer

24734209, 0, Downloaded from https://aapm.onlinelibrary.wiley.com/doi/10.1002/mp.16987 by IRCCS Centro di Riferimento Oncologi (CRO) Aviano (Pordenone), Wiley Online Library on [18/01/2024]. See the Terms and Conditions (https://onlinelibrary.wiley.com/terms-and-conditions) on Wiley Online Library for rules of use; OA articles are governed by the applicable Creative Commons License

recommended that plugs between −100 and +100 HU should not be used and that the measured CT number of real water should be used. Furthermore, the entire ρ for adipose/muscle was underestimated for Tomotherapy because the CT-ρ of the real water (CT number: 0 HU, ρ: 1.0 g/cm^3) was lower than that obtained from the calibration curve based on human tissue (Figure 7). The average $\Delta\rho_m$ value for adipose/muscle was 2.1% for Tomotherapy TPSs, which is comparable to the target dose difference of 1%–2% for prostate cancer.[11]

Dosimetry audits for density inhomogeneity were implemented through end-to-end tests with an anthropomorphic or inhomogeneous phantom.[2,3,5] If the dose deviation at their institute exceeded the tolerance level of the dosimetry audit, the participating institutes attempted to detect the cause. However, it is impossible to evaluate the CT-ρ and CT-ρ_e calibration errors from the end-to-end test results. Furthermore, because dosimetry audit phantoms for inhomogeneity constitute only a few tissue-equivalent plastics, heterogeneity correction in the human body, consisting of lung, adipose, muscle, spongy bone, and cortical bone, has not been verified for all tissues. Conversely, the dose calculation algorithm has also not been verified for a CT number calibration audit. Therefore, heterogeneity correction can be comprehensively verified for all tissues by combining dosimetry and CT number calibration audits.

The CT number calibration audit in this study was independent of TPS, dose calculation algorithm, and phantom manufacturer, and institute-specific CT number calibration curves were compared with the theoretical CT number calibration curve. Thus, two of the 24 participating institutes found that the ρ_e values in the catalog were registered in the TPS and re-registered more accurate ρ_e values described in the TEM specification. Once institute-specific CT number calibration curve was registered in the TPS, the ρ and ρ_e of the TEMs are less frequently reviewed for consistency with the manufacturer's specifications. Therefore, the CT number calibration audit provided an opportunity to review institute-specific CT number calibration curves.

A limitation of this study is that the tolerance levels could be defined as too simple to estimate the dose error caused in the human body. The tolerance levels were established to cause a 2% dose error at the effective tissue thickness and tissue maximum ratio with a 10 cm × 10 cm field. Thus, even if the $\Delta\rho_{TEM}$ and $\Delta\rho_{e,TEM}$ exceeded the tolerance levels, this did not mean that they caused 2% dose error in the human body.

5 | CONCLUSIONS

For the first time, we assessed CT number calibration curves for the ρ and ρ_e created by 24 Japanese photon therapy institutes. Latent deviations between human tissues and TEMs were determined by comparing the CT number calibration curves obtained from multiple institutes. A high tissue-equivalent CT number calibration curve was created using numerous TEMs, even if some TEMs registered in the TPS exceeded the tolerance levels. The CT-ρ calibration curves for the adipose/muscle region for Tomotherapy were created using water only, according to the manufacturer's recommendations, emphasizing the difference between human tissue and real water. The CT number calibration audit provides an opportunity to review institute-specific CT number calibration curves and is useful for reducing CT number calibration errors. While dosimetry audits for density inhomogeneity have been implemented using anthropomorphic or inhomogeneous phantoms, these methods have certain limitations. In particular, end-to-end tests are unable to evaluate CT-ρ and CT-ρ_e calibration errors and does not cover all tissue types of the human body. Conversely, the dose calculation algorithm has not been evaluated using a CT number calibration audit. Therefore, it is suggested that a comprehensive verification of the heterogeneity correction for all tissues can be achieved by combining dosimetry and CT number calibration audits.

ACKNOWLEDGMENTS

We thank Dr. Hiroto Munetsuna from the Hiroshima Prefectural Technology Research Institute for his technical support in the elemental weight measurements. We thank the photon therapy institutes that participated in the audits. This work was supported by the Japan Agency for Medical Research and Development (AMED) under grant number 2031526, the National Cancer Center Research and Development Fund: 2020-J-3, and the Japan Society for the Promotion of Science (JSPS) KAKENHI grant numbers 19K12865 and 23K14869.

CONFLICT OF INTEREST STATEMENT

The authors declare no conflicts of interest.

REFERENCES

1. Giacometti V, Hounsell AH, McGarry CK. A review of dose calculation approaches with cone beam CT in photon and proton therapy. *Phys Med*. 2020;76:243-276.
2. Nishio T, Shirato H, Ishikawa M, et al. Design, development of water tank-type lung phantom and dosimetric verification in institutions participating in a phase I study of stereotactic body radiation therapy in patients with T2N0M0 non-small cell lung cancer: Japan Clinical Oncology Group trial. *J Radiat Res*. 2014;55:600-607.
3. Lye J, Kenny J, Lehmann J, et al. A 2D ion chamber array audit of wedged and asymmetric fields in an inhomogeneous lung phantom. *Med Phys*. 2014;41:101712.
4. Clark CH, Aird EG, Bolton S, et al. Radiotherapy dosimetry audit: three decades of improving standards and accuracy in UK clinical practice and trials. *Br J Radiol*. 2015;88:20150251.
5. Lehmann J, Alves A, Dunn L, et al. Dosimetric end-to-end tests in a national audit of 3D conformal radiotherapy. *Phys Imaging Radiat Oncol*. 2018;6:5-11.

24734209, 0, Downloaded from https://aapm.onlinelibrary.wiley.com/doi/10.1002/mp.16987 by IRCCS Centro di Riferimento Oncologi (CRO)- Aviano (Pordenone), Wiley Online Library on [18/01/2024]. See the Terms and Conditions (https://onlinelibrary.wiley.com/terms-and-conditions) on Wiley Online Library for rules of use; OA articles are governed by the applicable Creative Commons License

6. Peters LJ, O'Sullivan B, Giralt J, et al. Critical impact of radiotherapy protocol compliance and quality in the treatment of advanced head and neck cancer: results from TROG 02.02. *J Clin Oncol*. 2010;28:2996-3001.
7. Peters N, Wohlfahrt P, Dahlgren CV, et al. Experimental assessment of inter-centre variation in stopping-power and range prediction in particle therapy. *Radiother Oncol*. 2021;163:7-13.
8. Hatton J, McCurdy B, Greer PB. Cone beam computerized tomography: the effect of calibration of the Hounsfield unit number to electron density on dose calculation accuracy for adaptive radiation therapy. *Phys Med Biol*. 2009;54:329-346.
9. Guan H, Dong H. Dose calculation accuracy using cone-beam CT (CBCT) for pelvic adaptive radiotherapy. *Phys Med Biol*. 2009;54:6239-6250.
10. Disher B, Hajdok G, Wang A, Craig J, Gaede S, Battista JJ. Correction for "artificial" electron disequilibrium due to cone-beam CT density errors: implications for on-line adaptive stereotactic body radiation therapy of lung. *Phys Med Biol*. 2013;58:4157-4174.
11. Tsunemine S, Ozawa S, Nakao M, et al. Tolerance levels of mass density for adaptive helical tomotherapy using MVCT. *J Radiat Res*. 2023;64:195-201.
12. Davis AT, Palmer AL, Nisbet A. Can CT scan protocols used for radiotherapy treatment planning be adjusted to optimize image quality and patient dose? A systematic review. *Br J Radiol*. 2017;90:20160406.
13. Nakao M, Ozawa S, Yamada K, et al. Tolerance levels of CT number to electron density table for photon beam in radiotherapy treatment planning system. *J Appl Clin Med Phys*. 2018;19:271-275.
14. Nakao M, Ozawa S, Yogo K, et al. Tolerance levels of mass density for CT number calibration in photon radiation therapy. *J Appl Clin Med Phys*. 2019;20:45-52.
15. Jacobsen MC, Thrower SL, Ger RB, et al. Multi-energy computed tomography and material quantification: current barriers and opportunities for advancement. *Med Phys*. 2020;47:3752-3771.
16. McGarry CK, Grattan LJ, Ivory AM, et al. Tissue mimicking materials for imaging and therapy phantoms: a review. *Phys Med Biol*. 2020;65:23TR01.
17. Schneider U, Pedroni E, Lomax A. The calibration of CT Hounsfield units for radiotherapy treatment planning. *Phys Med Biol*. 1996;41:111-124.
18. Schneider W, Bortfeld T, Schlegel W. Correlation between CT numbers and tissue parameters needed for Monte Carlo simulations of clinical dose distributions. *Phys Med Biol*. 2000;45:459-478.
19. Ödén J, Zimmerman J, Bujila R, Nowik P, Poludniowski G. Technical note: on the calculation of stopping-power ratio for stoichiometric calibration in proton therapy. *Med Phys*. 2015;42:5252-5257.
20. Ödén J, Zimmerman J, Poludniowski G. Comparison of CT-number parameterization models for stoichiometric CT calibration in proton therapy. *Phys Med*. 2018;47:42-49.
21. ICRP, 1975. Report. Report of the Task Group on Reference Man. ICRP Publication 23.
22. ICRU Report 44, Tissue Substitutes in Radiation Dosimetry and Measurement. 1989.
23. ICRU Report 46, Photon, Electron, Proton, and Neutron Interaction Data for Body Tissues; 1992.
24. ICRP. 2009. Adult Reference Computational Phantoms. ICRP Publication 110. *Ann. ICRP* 39(2).
25. Nakao M, Ozawa S, Miura H, et al. Development of a CT number calibration audit phantom in photon radiation therapy: a pilot study. *Med Phys*. 2020;47:1509-1522.
26. Inaniwa T, Tashima H, Kanematsu N. Optimum size of a calibration phantom for x-ray CT to convert the Hounsfield units to stopping power ratios in charged particle therapy treatment planning. *J Radiat Res*. 2018;59:216-224.
27. ISO 845. Cellular plastics and rubbers, Determination of apparent density. 2006; 1-4.
28. Nakao M, Hayata M, Ozawa S, et al. Stoichiometric CT number calibration using three-parameter fit model for ion therapy. *Phys Med*. 2022;99:22-30.
29. Kanematsu N, Inaniwa T, Nakao M. Modeling of body tissues for Monte Carlo simulation of radiotherapy treatments planned with conventional x-ray CT systems. *Phys Med Biol*. 2016;61:5037-5050.
30. Cheung JP, Shugard E, Mistry N, Pouliot J, Chen J. Evaluating the impact of extended field-of-view CT reconstructions on CT values and dosimetric accuracy for radiation therapy. *Med Phys*. 2019;46:892-901.
31. Fonseca GP, Baer-Beck M, Fournie E, et al. Evaluation of novel AI-based extended field-of-view CT reconstructions. *Med Phys*. 2021;48:3583-3594.
32. Davis AT, Palmer AL, Pani S, Nisbet A. Assessment of the variation in CT scanner performance (image quality and Hounsfield units) with scan parameters, for image optimisation in radiotherapy treatment planning. *Phys Med*. 2018;45:59-64.
33. Hudobivnik N, Schwarz F, Johnson T, et al. Comparison of proton therapy treatment planning for head tumors with a pencil beam algorithm on dual and single energy CT images. *Med Phys*. 2016;43:495-504.
34. Gomà C, Almeida IP, Verhaegen F. Revisiting the single-energy CT calibration for proton therapy treatment planning: a critical look at the stoichiometric method. *Phys Med Biol*. 2018;63:235011.

SUPPORTING INFORMATION

Additional supporting information can be found online in the Supporting Information section at the end of this article.

How to cite this article: Nakao M, Ozawa S, Miura H, et al. CT number calibration audit in photon radiation therapy. *Med Phys*. 2023;1-12. https://doi.org/10.1002/mp.16887

24734209, 0, Downloaded from https://aapm.onlinelibrary.wiley.com/doi/10.1002/mp.16887 by IRCCS Centro di Riferimento Oncologi (CRO) - Aviano (Pordenone), Wiley Online Library on [18/01/2024]. See the Terms and Conditions (https://onlinelibrary.wiley.com/terms-and-conditions) on Wiley Online Library for rules of use; OA articles are governed by the applicable Creative Commons License